US-TAIWAN COLLABORATIVE RESEARCH ON STEEL COLUMN THROUGH CYCLIC TESTING OF TWO-STORY SUBASSEMBLAGES

C. C. Chou[(1)], T. H. Lin[(2)], Y. C. Lai[(3)], H. C. Xiong[(4)],
C. M. Uang[(5)], S. El-Tawil[(6)], J. P. McCormick[(7)], G. Mosqueda[(8)]

[(1)]*Professor, Dept. of Civil Engineering, National Taiwan University, Taiwan, cechou@ntu.edu.tw*
Head, Building Engineering Division, National Center for Research on Earthquake Engineering (NCREE), Taiwan
[(2)]*Ph. D. Student Researcher, Dept. of Civil Engineering, National Taiwan University, thlin@ncree.narl.org.tw*
Assistant Researcher, National Center for Research on Earthquake Engineering (NCREE), Taiwan
[(3)]*Graduate Student Researcher, Dept. of Civil Engineering, National Taiwan University, Taiwan, r07521232@ntu.edu.tw*
[(4)]*Graduate Student Researcher, Dept. of Civil Engineering, National Taiwan University, Taiwan, r07521238@ntu.edu.tw*
[(5)]*Professor, Dept. of Structural Engineering, University of California, San Diego, USA, cmu@ucsd.edu*
[(6)]*Professor, Dept. of Civil and Environmental Engineering, University of Michigan, Ann Arbor, USA, eltawil@umich.edu*
[(7)]*Professor, Dept. of Civil and Environmental Engineering, University of Michigan, Ann Arbor, USA, jpmccorm@umich.edu*
[(8)]*Professor, Dept. of Structural Engineering, University of California, San Diego, USA, gmosqueda@ucsd.edu*

Abstract

Recent studies showed that the seismic performance of steel columns is affected by the boundary conditions at both ends of the member. To reflect realistic boundary conditions, five half-scale, two-story steel subassemblage frames with a single column and steel beams at two floors were tested to evaluate the cyclic behavior of steel columns. The prototype design was based on a seven-story apartment building in Taiwan. The building is a dual system with a special moment-resisting frame (SMRF) and a buckling-restrained braced frame (BRBF). Three subassemblages (Specimens HC-37, HC-37-R and HC-49) used H-shaped columns of SN490B steel, the difference being that the web depth-to-thickness ratio (=49) of the last specimen was higher than that (37) of the first two specimens. The remaining two subassemblages (Specimens HBC-12 and HBC-16) used built-up box columns of SM570M steel; the wall width-to-thickness ratios were 12 and 15.7, respectively. The same built-up I-shaped beams of SN490B steel with a Reduced Beam Section (RBS) were used for all five subassemblies. A constant axial compression force ranging from 20 and 40% of the column yield force was applied to the column; the top end of the column was cyclically loaded with a sequence of increasing lateral drifts. Test results showed that the realistic boundary condition at the top end of the first-story column significantly altered the moment distribution along the column height; such distribution was further affected by the column buckling at the bottom end. The H-shaped columns experienced much significant local buckling and axial shortening than the built-up box columns. The highly ductile member requirement in AISC 341 cannot assure a satisfactory seismic performance of the two H-shaped columns at a story drift angle of 0.04 rad, which is not the case for built-up box columns.

Keywords: High-Strength Steel, H-Shaped Column, Built-Up Box Column, Two-Story Subassemblage Frame Test, Column Inflection Point

1. Introduction

Steel H-shaped column (HC) and hollow box columns (HBC) are widely used in steel structural buildings. The HC and HBC, fabricated by welding plates, are similar to a wide-flange column and a hollow structural section (HSS) column, respectively. Several experiments have been conducted to characterize the hysteretic behavior of HCs and HBCs under cyclic loading; the studies showed that their seismic performances are strongly influenced by the member compactness, the amount of axial force, and the material yield strength, not concrete infill. However, the AISC 341 [1], AIJ [2] or Taiwan Code [3] have significantly different width-to-thickness (*b/t*) requirements for highly ductile members, leading to different column sections in design in a high seismic area [4].

To characterize the post-peak strength deterioration of HC and HBC specimens, researchers have investigated their seismic performances with different *b/t* and P/P_y ratios, where P is an applied axial compression force to a column and P_y is an axial yield force of a column. Many column tests are conducted using a fixed boundary condition at both ends [5-10]. However, the top end of the first-story column in a building is connected to beams and a column, which is not the same boundary condition as used in the typical test setup. Recent studies showed that the seismic performance of steel columns is affected by the boundary conditions at both ends. Elkady and Lignos [8] conducted tests for steel columns with a flexible or fixed boundary condition. To simulate the flexible boundary condition, a predefined rotation is applied to the top end of column specimens. The story drift angle when the column cannot maintain 0.9 times the maximum moment slightly moves from 0.022 to 0.026 rad. Wu et al. [9] conducted different finite element models using W24 column sections. The study showed that the columns with a spring-fixed boundary condition generally have a 0.01 rad higher angle capacity than those with a fixed-fixed boundary condition. Therefore, this work was aimed to test first-story steel columns using a realistic boundary condition. Five half-scale, two-story steel subassemblage frames with beams and a single column were planned in the US-Taiwan collaborative research, funded by the Ministry of Science and Technology, Taiwan and the National Institute of Standards and Technology, USA. This paper presents preliminary test results of the five two-story steel subassemblages; these tests were conducted at NCREE, Taiwan before the end of 2019.

2. Prototype and Subassemblage Frames

The prototype frame structure is a seven-story apartment building using buckling-restrained braces, BRBs [11-14], which uses columns of SM570MC steel with the nominal yield strength of 420 MPa and I-shaped beams and BRBs of SN490B steel with the nominal yield strength of 325 MPa. The design details of the prototype frame can be found in Lin et al. [15]. Fig. 1(a) shows the elevation of the prototype. A half-scale subassemblage frame is a two-and-half story frame that consists of a center column and beams at two floors, marked in Fig. 1(a). The height and width of the test frame are 4.625 and 4 m, respectively. Table 1 lists the beam and column sections.

Two setup schemes for the subassemblage frame test were studied. Fig. 1(b) shows a Scheme A model, which needs five actuators. One actuator controls the lateral displacement of the column, and four actuators control the movement of the second and third floor beams. Fig. 1(c) shows a Scheme B model, which needs three actuators and simplifies the test setup work. One actuator controls the lateral displacement of the column. Two actuators control the movement of the third floor beam, and two rigid links are connected between the second and third floor beams to maintain a relative story height during the test. The following summarizes the time history analysis results of the prototype frame and two scheme models under two ground motions.

Table 1. Beam and column sections of the prototype and subassemblage

	Prototype frame (unit: mm)	Subassemblage frame (unit: mm)	Material
Center Column	Box 385×385×28	Box 192.5×192.5×14	SM570MC (F_{ny}=420 MPa)
Beam	I 512×202×12×25	I 256×101×6×12.5	SN490B (F_{ny}=325 MPa)

Table 2. Characteristics of two ground motions

Event	Type	Year	Station	PGA (gal)	PGV (cm/sec)	Scaled PGA (gal)
Kobe	Far field	1995	ABN090	230	24	1098
Landers	Near fault	1992	Lucerne-260	711	134	1203

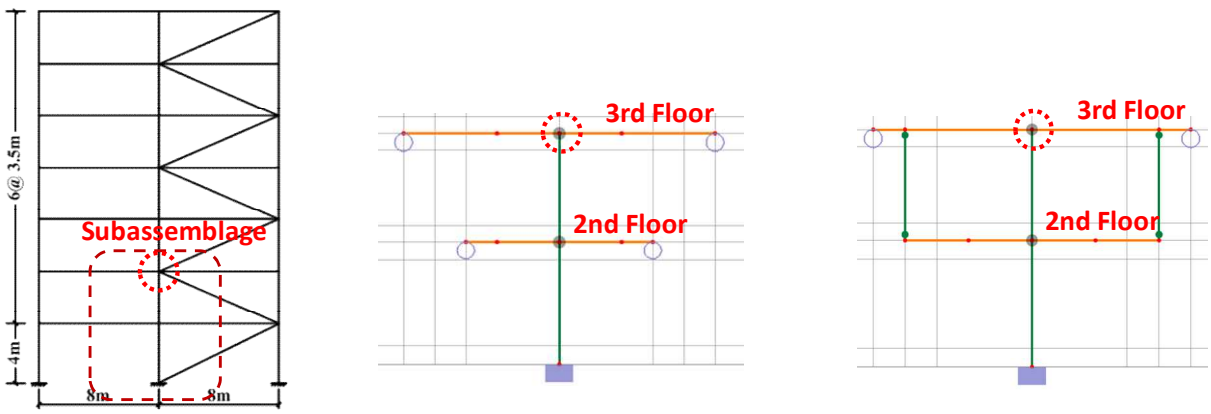

(a) Prototype (b) Scheme A (c) Scheme B

Fig. 1. Elevation of the prototype frame and two test schemes

2.1 Analytical Models and Results

The seven-story prototype frame structure and the frame specimen, which has a center column and beams at two floors [Fig. 1 (b) and (c)], were modeled using the computer program, PISA3D [16]. The damping ratio of the steel frame was 3%. The bilinear plastic hinge of the columns and beams were modeled according to Chapter 9, ASCE 41 [17]. The axial force on the center and outer columns were $0.25P_y$ and $0.2P_y$, respectively, based on the design of the prototype frame. Two earthquake records were used for the nonlinear time history analyses of the frames. The first record was a far-field earthquake motion in Kobe, 1995; the second record was a near-fault earthquake motion in California, 1992. The original records were scaled to match the maximum-considered earthquake (MCE) design spectrum of the prototype building. Table 2 lists the ground motion data, peak ground acceleration (PGA), peak ground velocity (PGV), and scaled peak ground acceleration (PGA).

Fig. 2 shows the time history analysis results of the prototype subjected to Kobe and Landers motions. The legends of RBC, CBC and LBC represent right, center and left columns, respectively. The maximum story drift angles at the second and third floors are about 0.02 and 0.04 rad for the prototype frame under the Kobe and Landers motions, respectively. The third-floor displacement history and the center-column axial force history of the prototype were applied to the center column of two scheme models, marked by a red dashed circle [Fig. 1(b) and (c)]. Fig. 3 shows the comparison of the shear force and moment of the first-story column obtained from the prototype frame, scheme models A and B under the Kobe motion. The inelastic time history analyses of the two scheme models under the applied axial force and displacement histories show similar results as the prototype frame under the ground motion. Therefore, the Scheme B was determined for the two-story subassemblage test.

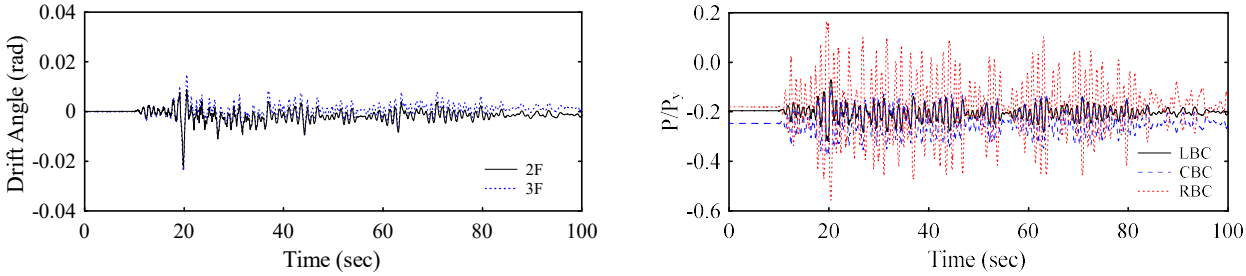

(a) Kobe (far field motion)

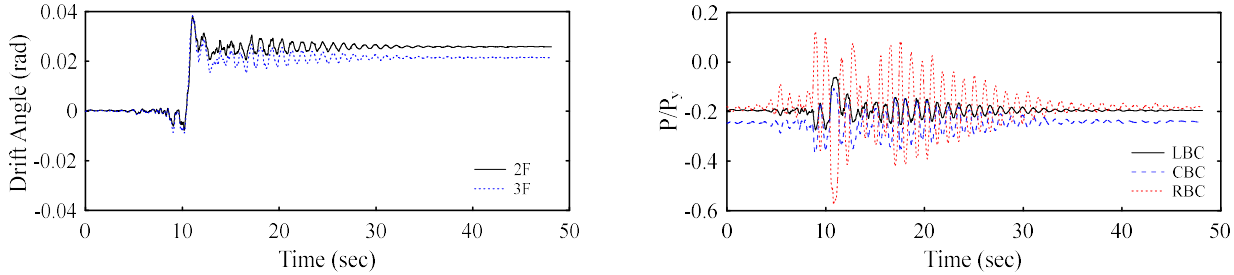

(b) Landers (near fault motion)

Fig. 2. Story drift angle and axial force ratio of the prototype frame (MCE level)

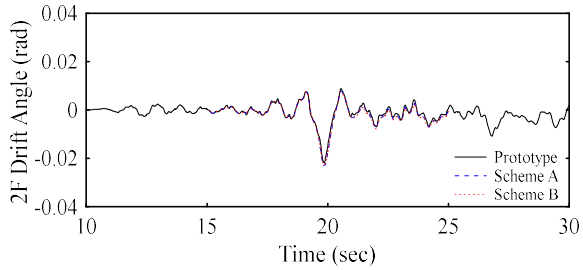

(a) Second-story drift angle

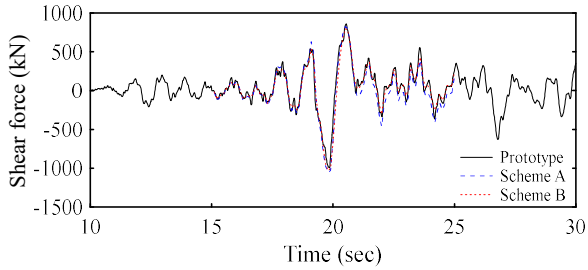

(b) Shear force of the first-story CBC

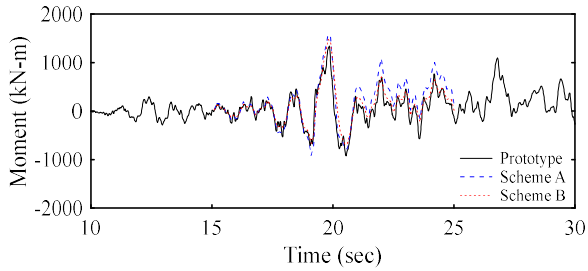

(c) Moment at top end of the first-story CBC

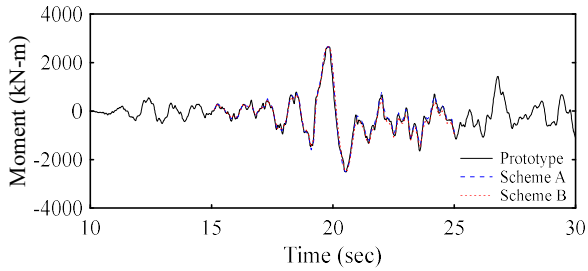

(d) Moment at base of the first-story CBC

Fig. 3. Time history analysis of all frames under Kobe motion

3. Tests of Half-Scale, Two-Story Steel Subassemblages

Five subassemblage specimens were planned for the experimental program. Table 3 lists the column size and properties of the subassemblage specimens. All columns satisfy the compactness limits for highly ductile members in AISC 341 [1] except for Specimen HBC-16, which still meets the most compact section in AIJ [2] and Taiwan code [3]. Moreover, Specimen HC-49 has a web compactness ratio, h/t_w, of 49.3, slightly

lower than the limit (=51.4) for highly ductile members [1]. Fig. 4 shows the elevation of Specimen HC-37, which is a two-and-half story steel frame. An axial force controlling system, which has hydraulic jacks and prestressing bars, was used to apply axial compressive forces at the top end of the column. Two rigid links that connected the outer part of the third-floor and second-floor beams were used to maintain a relative story height during the test. Load cells were positioned at the top end of the rigid link in order to obtain shear forces in the second-floor beams. The axial shortening of the steel column was expected during testing and the vertical movement of the beam ends, attached to actuators, was controlled to be the same as the measured shortening of the column. The second-floor beam end displacements were subjected to the same vertical displacement by rigid links, attached to the third-floor beams. Four lateral supports were adopted to minimize the out-of-plane movement of the subassemblage frame. The top end of the column was cyclically loaded with a sequence of increasing lateral drifts, similar to the loading protocol for moment connections in AISC 341 [1].

Fig. 5 shows the lateral force versus lateral displacement response of subassemblage specimens; the frame drift angle is defined as the horizontal actuator displacement divided by a total column height of 4620 mm (Fig. 4) and is used as a controlling parameter for the test. Since the axial compression force is applied to all specimens, the first-story moment at the base, M, is computed by considering a free-body diagram of the two-story subassemblage:

$$\begin{aligned} M = {} & \left[L_{H,Act}\left(F_{H,Act}\cos\theta_{H,Act}\right) - \left(L_{H,Act} + L_{Top}\right)\left(P\sin\theta_{Top}\right)\right] \\ & + \left[\left(P\cos\theta_{Top} + F_{H,Act}\sin\theta_{H,Act}\right)\left(\delta_{H,Act}\frac{L_{H,Act} + L_{Top}}{L_{H,Act}}\right)\right] \\ & + \left[\left(L_{3F,B}\cos\theta_{VS,Act}\right)F_{VS} - \left(L_{3F,B}\cos\theta_{VN,Act}\right)F_{VN}\right] \end{aligned} \quad (1)$$

where $L_{H,Act}$ is the height of the horizontal actuator, $F_{H,Act}$ is the horizontal actuator force, $\theta_{H,Act}$ is the angle of the horizontal actuator, $\theta_{VS,Act}$ is the angle of the South actuator, $\theta_{VN,Act}$ is the angle of the North actuator, P is the axial force on the column, F_{VS} is the South actuator force, F_{VN} is the North actuator force, $L_{3F,B}$ is the distance between the column centerline and the vertical actuator, $\delta_{H,Act}$ is the lateral movement of the column top end, θ_{Top} is the rotation of the column.

3.1 H-Shaped Column Response

Specimens HC-37, HC-37-R, and HC-49 that satisfy the highly ductile member requirement in AISC 341 [1] are subjected to a constant axial force of $0.2P_y$ (Table 3) before applying a lateral displacement at the column top end. At a frame drift angle of 0.025 rad, Specimen HC-37 exhibited minor column web and flange local buckling near the base. During the excursion of -0.035 rad frame drift angle, the lateral support was slightly moved because of friction against beams. The behavior was not observed in positive loading; the maximum lateral strength occurred at the first cycle of +0.035 rad frame drift angle and then degraded in the second cycle due to local buckling near the column base. Fig. 6(a) shows the deformation of the first-story column at a frame drift angle of 0.045 rad, the column being anti-symmetric flange buckling with local buckling amplitudes of 74 and 105 mm on North and South sides, respectively. The second-floor RBS showed significant yielding and slightly twisted. During the second cycle of 0.055 rad frame drift angle, the South second-floor beam fractured through the top flange near the groove weld joint, and the North second-floor beam showed significant web buckling and minor flange buckling.

Since the friction was observed between the lateral support and the specimen, a Teflon pad was used at all interfaces between the beam and the lateral support to eliminate friction for subsequent tests. At a frame drift angle of 0.02 rad, Specimen HC-49 showed minor web local buckling near the column base, which occurred earlier than Specimen HC-37. The maximum lateral strength was reached at a frame drift angle of 0.025 rad [Fig. 5(a)] with clear web and flange buckling near the column base; the buckling amplitude was about 10 mm. Specimen HC-49 showed strength degradation at a frame drift angle of 0.035 rad. At a 0.045 rad frame drift angle, the maximum flange buckling amplitude was about 75 and 85 mm on North and South sides, respectively; the web buckling amplitude was about 60 mm [Fig. 6(b)]. The second-floor RBS yielded and twisted with web a buckling amplitude of 10 mm. The post-peak lateral force of the subassemblage decreased 10% at a frame drift angle of 0.045 rad; the test was stopped after completing two cycles due to

significant column buckling near the base. The beam had no weld fracture or flange local buckling at the end of the test.

Specimen HC-37-R was composed of a top portion of Specimen HC-37 column and Specimen HC-49 beams, which did not fracture at the end of Specimen HC-49 test. Specimen HC-37-R was subjected to the same loading protocol as other specimens, but the jagged response as seen in Specimen HC-37 test was eliminated. The hysteretic response and observed performance of Specimens HC-37-R and HC-37 were very similar with strength degradation in a second cycle of a frame drift angle of 0.035 rad. During the first cycle of 0.055 rad frame drift angle, the second and third floor beams had web and flange buckling. The column and beam fractured in the second cycle of 0.055 rad frame drift angle [Fig. 5(b) and Fig. 6(c)], causing a significant strength degradation.

3.2 Built-Up Box Column Response

Specimens HBC-12 and HBC-16 were built-up box columns, subjected to $0.4P_y$ (=1643 kN) before applying the same lateral displacement as others. The beam and column base of Specimen HBC-12 yielded at frame drift angles of 0.01 and 0.02 rad, respectively. At a frame drift angle 0.025 rad, Specimen HBC-12 exhibited minor web and flange local buckling near the column base. The bottom end of the second-story column on the North side yielded at a drift angle of 0.035 rad, leading to un-symmetric deformation of the column. In positive loading, the lateral deformation of the second-story column was larger than that of the first-story column, but in negative loading, the first-story column deformed more than the second-story column. At a drift angle of -0.035 rad, the first-story column experienced flange buckling with an amplitude of 5 mm; the web buckling was also found on the second floor beam, but no strength degradation of the subassemblage frame was found. During the excursion from -0.045 to +0.055 rad drift angle, the third-floor South beam fractured, leading to significant strength degradation as shown in Fig. 5(c). Meanwhile, the lateral deformation of the first-story column did not increase with the increase of the actuator lateral displacement. When the subassemblage was moved to -0.055 rad frame drift angle, the first-story column reached a story drift angle of -0.08 rad [Fig. 6(d)] with no strength degradation.

Specimen HBC-16 showed column yielding and buckling at frame drift angles of 0.0145 and 0.025 rad, respectively. The amplitude of the flange local buckling was about 3 mm, right above stiffeners at the column base, in the first cycle of a frame drift angle of 0.045 rad. The third-floor South beam fractured during the first excursion to a frame drift angle of -0.045 rad, leading to a strength degradation [Fig. 5(d)] and un-symmetric deformation of the column, as seen in Specimen HBC-12 test [Fig. 6(d)]. The crack was found near the cope hole and flange of the third-floor North beam during the second cycle of a frame drift angle of 0.045 rad, leading to minor strength degradation. After unloading to about zero force, the South actuator was detached from the beam in order to condcut an exterior column test with only North beams. During the second cycle of a frame drift angle of -0.045 rad, the horizontal actuator force dropped 70 kN compared to the previous cycle [Fig. 5(d)]. The bottom flange of the third-floor North beam fractured in the first excursion to a frame drift angle of +0.055 rad. Although the lateral strength of the subassemblage frame decreased due to beam fracture, the axial force, $0.4P_y$, on the column was maintained throughout the test.

Table 3. Test matrix of five subassemblage specimens

	HC-37, HC 37-R	HC-49	HBC-12	HBC-16	Beam
Section	H-Shaped Column 320×160×8×12	H-Shaped Column 320×160×6×12	Box Column 190×190×13	Box Column 230×230×13	I-Shaped Beam 256×101×6×12
b/t (Flange)	6.7 (7.4)	6.7 (7.4)	12.6 (13.9)	15.7 (13.9)	4.2
h/t_w (Web)	37 (51.4)	49.3 (51.4)	12.6 (13.9)	15.7 (13.9)	38.7
Material	SN490B	SN490B	SM570MB	SM570MB	SN490B
P/P_y	0.2	0.2	0.4	0.4	0
M_p (kN-m)	279	260	273	410	136
M_y (kN-m)	251	234	184	277	119

(): Compactness limit for highly ductile members based on AISC 341 (2016)

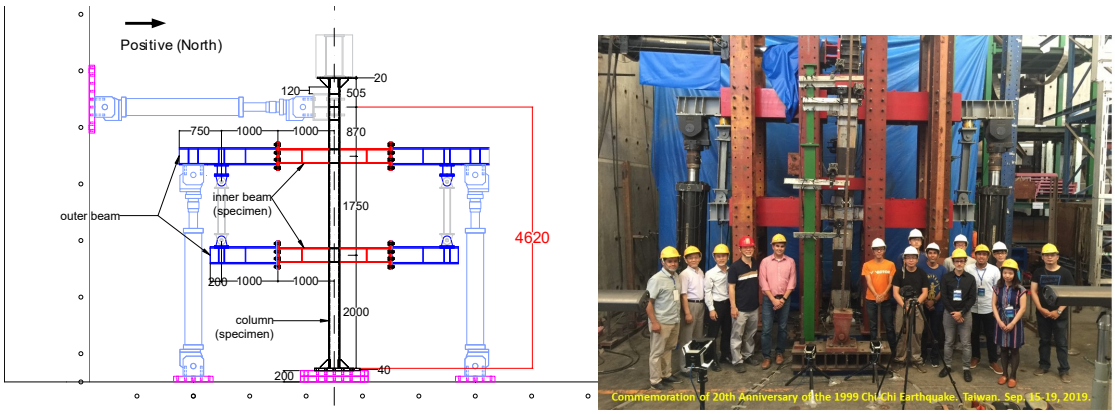

Fig. 4. Elevation of the subassemblage frame (unit: mm)

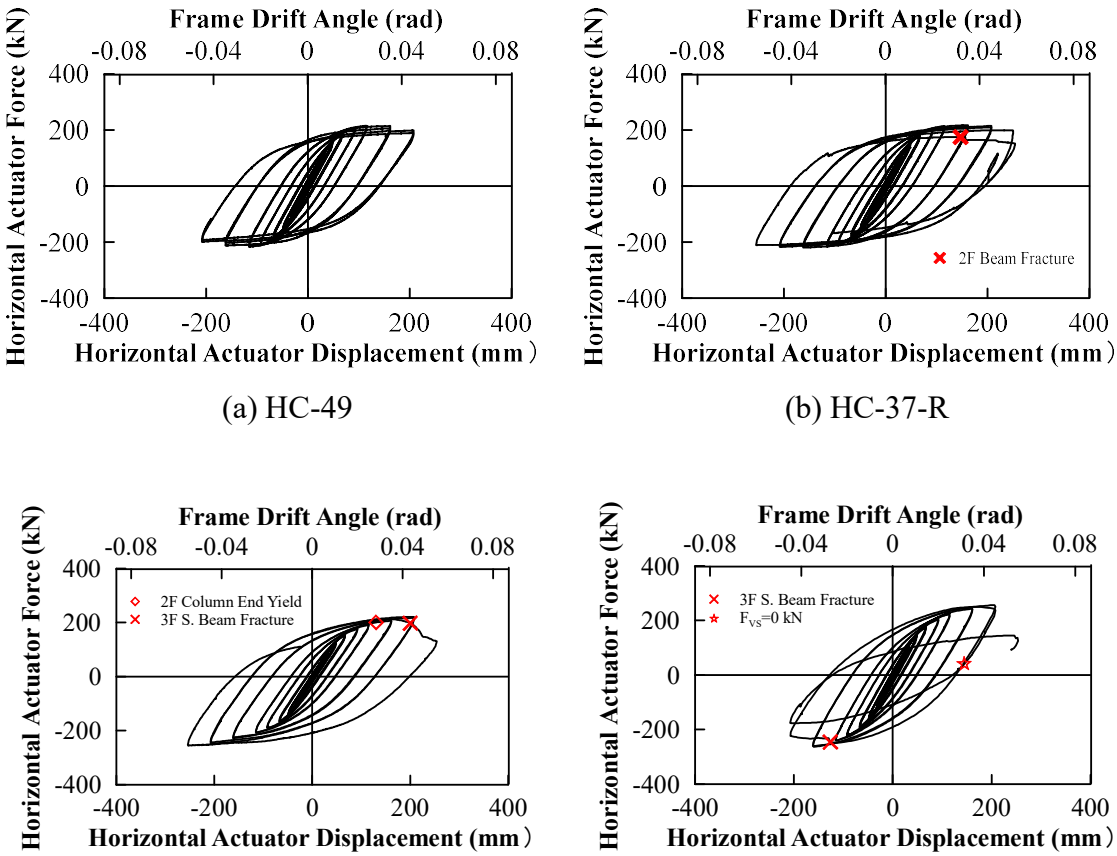

(a) HC-49 (b) HC-37-R

(c) HBC-12 (d) HBC-16

Fig. 5 Horizontal actuator force versus lateral displacement response

(a) HC-37 (0.045 rad) (b) HC-49 (0.045 rad) (c) HC-37-R (0.055 rad) (d) HBC-12 (-0.055 rad)

Fig. 6 First-story column performance

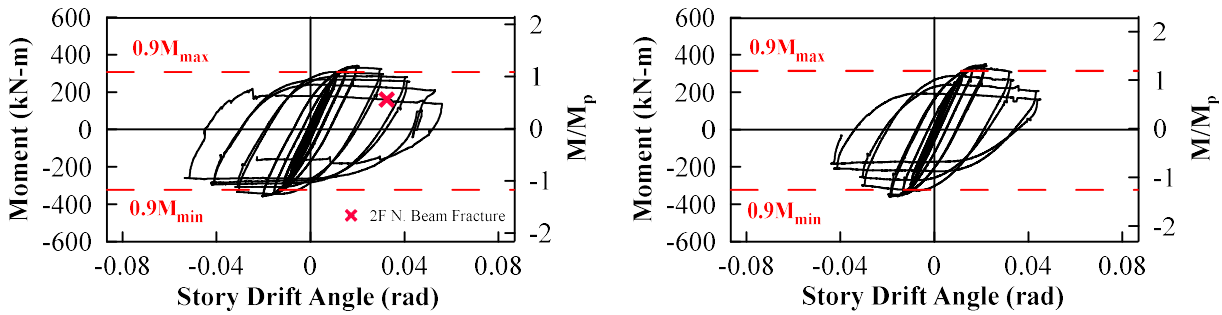

(a) HC-37-R

(b) HC-49

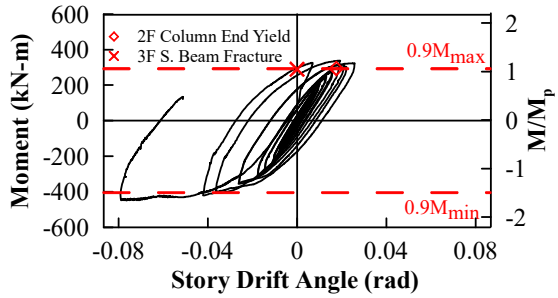

(c) HBC-12

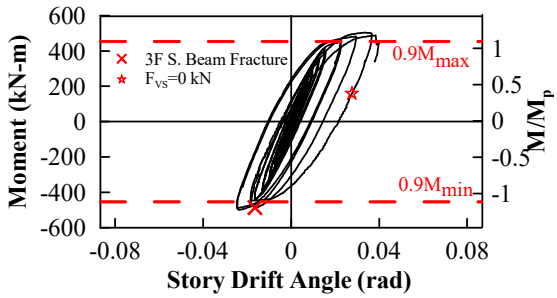

(d) HBC-16

Fig. 7 First-story column base moment versus story drift angle response

3.3 Column Base Moment and Inflection Point

Fig. 7 shows the column moment at the base versus the story drift angle, which was calculated by the second-floor displacement divided by the first-story height. All column specimens developed the plastic moment M_p (Table 3) at about a story drift angle of 0.01 rad. The H-shaped column developed the maximum moment, M_{max}, at a story drift angle of 0.02 rad and then exhibited strength degradation; Specimen HC-49 degraded faster than Speciemn HC-37-R [Fig. 7(a) and (b)] due to a larger h/t_w ratio. Speciemn HC-37-R

degraded below $0.9M_{max}$ during the first cycle of a story drift angle of 0.04 rad [Fig. 7(a)], but Specimen HC-49 degraded below $0.9M_{max}$ during the first cycle of a story drift angle of 0.03 rad [Fig. 7(b)]. The strength degradation of Specimen HC-49 was faster than that of Speicmen HC-37-R during a story drift angle of 0.04 rad, where all beams were in strain hardening level with minor web local buckling. If the post-peak strength ($0.9M_{max}$) of a column at a story drift angle of 0.04 rad is a required performance, these two H-shaped columns, which satisfy the highly ductile member requirement in AISC 341 [1], do not perform satisfactorily under an axial force of $0.2P_y$. However, Specimen HBC-12 under an axial force of $0.4P_y$ can perform well [Fig. 7(c)]; the beam facture and the second-story column yield lead to un-symmetric deforamtion of the first-story column to a story drift angle of -0.08 rad. No fracture or significant buckling was found near the column base.

The inflection point of a column represents a position of zero moment along the column height. Fig. 8 shows the moment distribution along the column height at different story drift angles. The flexural rigidity at the column base is much stiffener than that provided by the second-floor beams and column so all specimens exhibit the inflection point between 0.75 and 0.85 times the first-story height from the column base in the elastic response (i.e., 0.005 rad frame drift angle). The inflection point of the first-story column moves up with the increase of the lateral displacement (or lateral force) in the column pre-buckling stage, showing that the column base takes more moment than the column top end. The first-story column in the subassemblage frame does not have a fixed-fixed boundary condition, as typiclly used in a single column test. For H-shaped columns to develope the maximum strength at a story drift angle of 0.02 rad (pre-buckling stage), the inflection point also moves up to the highest position. Then, the infection point moves downward with the increase of column buckling near the base (post-buckling stage to a frame drift angle of 0.04 rad). The moment redistribution along the column height is further affected by the strength degradation at the column base [Fig. 8(a) and (b)]; the top end of the first-story column does not yield at the end of the test. However, the inflection points of the first-story box columns (Speciemns HBC-12 and HBC-16) continue to move up until the end of tests becasue the base with minor column local buckling still provides larger flexural stiffness than the second-floor beam-to-column connection [Fig. 8(c) and (d)]. The first-story box column deforms in a single curvature bending at a story drift angle of 0.04 rad.

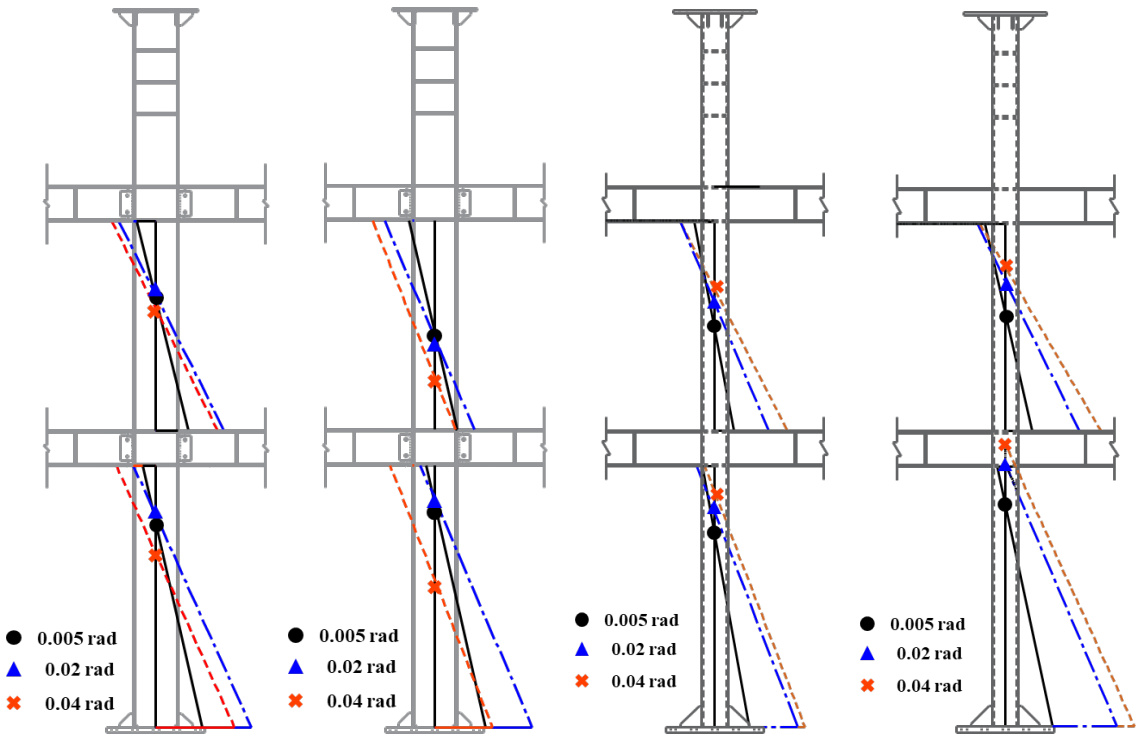

(a) HC-37-R (b) HC-49 (c) HBC-12 (d) HBC-16

Fig. 8 Column moment distribution and inflection point (drawn in scale)

4. Conclusions

Five two-story steel subassemblage frames with a single column and beams at two floors were tested to evaluate the effect of boundary conditions on the cyclic behavior of the first-story steel columns. Three subassemblages (Specimens HC-37, HC-37-R and HC-49) used H-shaped columns of SN490B steel, the difference being that the width-thickness ratio (=49) of the last specimen was higher than that (37) of the first two specimens. The remaining two subassemblages (Specimens HBC-12 and HBC-16) used built-up box columns of SM570M steel; the wall width-to-thickness ratios were 12 and 15.7, respectively. The same built-up I-shaped beams of SN490B steel with a Reduced Beam Section (RBS) were used for all five subassemblies. A constant axial compression force ranging from 20 and 40% of the yield force was applied to the column; the top end of the column was cyclically loaded with a sequence of increasing lateral drifts. Specimens HC-37, HC-37-R, HC-49, and HBC-12 satisfied the *b/t* limits for highly ductile members per AISC 341 [1], but Specimen HBC-16 violated this requirement. All two-story subassemblarges performed well at a frame drift angle of 0.04 rad (Fig. 5), but the columns with different compactness ratios and shapes showed different hyateretic responses (Fig. 7). All H-shaped columns exhibited web and flange local bukling near the base and showed a strength degradation beynod a story drift angle of 0.02 rad. Although the H-shaped columns satisfied the highly ductile member requirement in AISC 341, the post-peak strength degraded below $0.9M_{max}$ at 0.04 rad and 0.03 rad story drift angles for Specimens HC-37-R and HC-49, respectively, under an axial force of $0.2P_y$ [Fig. 7(a) and (b)]. However, the built-up box columns under an axial force of $0.4P_y$ did not exhibit a strength degradation throughout the test [Fig. 7(c) and (d)]. Specimen HBC-12 performed well at the last cycle to a story drift angle of 0.08 rad, which is similar to that reported by Chou and Chen [4] on a single column subjected to a near-fault loading.

The inflection point of the first-story column was between 0.75 and 0.85 times the first-story height from the column base in the ealstic response (Fig. 8), indicating that the second-floor beams and column do not provide the same flexural rigidity as the column base. For H-shaped column specimens, the inflection point moved upper as the column base developed much larger moment than the top end in the pre-buckling stage (i.e., before a first-story drift angle of 0.02 rad), and started to move downward in the post-peak buckling stage due to significant column buckling near the base [Fig. 8(a) and (b)]. Since the built-up box columns did not show a strength degradation, the inflection point of the first-story column always moved up until the end of the test, approaching to a single curvature bending [Fig. 8(c) and (d)]. The variation of the inflection point from the two-story subassemblage tests showed that (1) the first-story column does not behave as a fixed-fixed column, and (2) the amplitude of column buckling near the base significantly affects the moment distribution along the height of the column.

Acknowledgements

This cooperative research project among NCREE, National Taiwan University, University of California, San Diego, and University of Michigan, Ann Arbor is supported by the Ministry of Science and Technology, Taiwan. Additional support is provided by a funding from the National Institute of Standards and Technology, USA.

References

[1] ANSI, AISC 341-16. (2016). *Seismic provisions for structural steel buildings,* 60601.

[2] AIJ (2010). *Recommendation for limit state design of steel structures*. Architectural Institute of Japan.

[3] Taiwan Code (2010). *Design and technique specifications of steel structures for buildings*. Construction and Planning Agency Ministry of the Interior, Taiwan.

[4] Chou, C. C., Chen, G. W. (2020). "Cyclic lateral testing and backbone curve development of steel built-up hollow box columns in high axial load," *17th World Conference on Earthquake Engineering,* Paper No. C313, Sendai, Japan.

[5] Fadden, M., McCormick, J. (2011). "Cyclic quasi-static testing of hollow structural section beam members," *J. Structural Engineering*, ASCE, 138(5), 561-570.

[6] Chou, C. C., Wu, S. C. (2019). "Cyclic lateral load test and finite element analysis of high-strength concrete-filled steel box columns under high axial compression," *Engineering Structures*, 189, 89-99.

[7] Chou, C. C., Lee, C. S., Wu, K. Y., Chin, V. L. (2018). "Development and validation of a FRP-wrapped spiral corrugated tube for seismic performance of circular concrete columns," *Construction and Building Materials*, 170, 498-511.

[8] Elkady A., Lignos, D. G. (2018). "Full-scale testing of deep wide-flange steel columns under multi axis cyclic loading: loading sequence, boundary effects, and lateral stability bracing force demands," *J. Struct. Eng.*, ASCE, 144(2): 04017189.

[9] Wu, T. U., El-Tawil, S., McCormick, J. (2018). "Highly ductile limits for deep steel columns," *J. Struct. Eng.* 144 (4): 04018016.

[10] Ozkula, G., Harris, J., Uang, C. M. (2017). "Cyclic backbone curves for steel wide-flange columns: a numerical study," *EUROSTEEL*, Copenhagen, Denmark, 3365-3374.

[11] Chou, C. C., Chen, S. Y. (2010). "Subassemblage tests and finite element analyses of sandwiched buckling-restrained braces," *Engineering Structures*, 32(8), 2108-2121.

[12] Chou, C. C., Liu, J. H., Pham, D. H. (2012). "Steel buckling restrained braced frames with single and dual corner gusset connections: seismic tests and analyses," *Earthquake Engineering & Structural Dynamics*, 41(7), 1137-1156.

[13] Chou, C. C., Chung, P. T., Cheng, Y. T. (2016). "Experimental evaluation of large-scale dual-core self-centering braces and sandwiched buckling-restrained braces." *Engineering Structures,* 116, 12-25.

[14] Chou, C. C., Hsiao, C. H, Chen, Z. B, Chung, P. T, Pham, D. H. (2019). "Seismic loading tests of full-scale two-story steel building frames with self-centering braces and buckling-restrained braces," *Thin-Walled Structures*, 140, 168-181.

[15] Lin, T. H., Chou, C. C., Chen, G. W. (2019). "A seven-story steel braced frame under far-field and near-fault earthquakes: loading protocol and seismic test of high-strength steel H-shaped columns," *International Conference in Commemoration of 20th Anniversary of the 1999 Chi-Chi Earthquake.* Taiwan.

[16] Lin, B. Z., Chuang, M. C., Tsai, K. C. (2009). "Object-oriented development and application of a nonlinear structural analysis framework," *Advances in Engineering Software*, 40(1): 66-82.

[17] ASCE. 2014. *Seismic evaluation and retrofit of existing buildings*, ASCE 41-13. American Society of Civil Engineers, Virginia, USA.

